Jurnal Teknologi

Full Paper

THE EFFECT OF HEAT-TREATMENT ON THE MECHANICAL PROPERTIES OF EXPANDED GLASS PARTICLE/A356 SYNTACTIC FOAM

Kadhim Al-sahlani[a]*, Ahmed G. Hassan[b], Zainab Salim Hadawi[c]

[a]Mechanical Engineering Department, College of Engineering, University of Thi-Qar, 64001, Nasiriyah city, Iraq
[b]Biomedical Engineering Department, College of Engineering, University of Thi-Qar, 64001, Nasiriyah city, Iraq
[c]Chemistry Department, College of Science, University of Thi-Qar, 64001, Nasiriyah City, Iraq

Article history
Received
6 April 2024
Received in revised form
25 June 2024
Accepted
23 July 2024
Published Online
22 December 2024

*Corresponding author
kadimalsahlani@utq.edu.iq

Grahical abstract

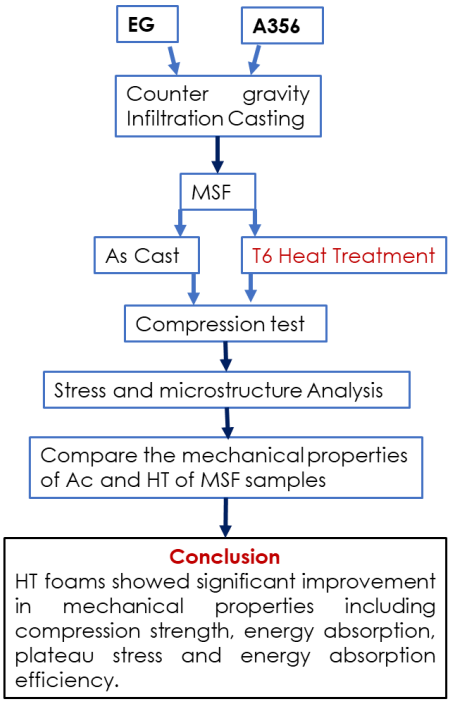

Abstract

This research investigates the manufacturing of metal syntactic foams (MSFs) using a packed bed of porous (2-2.8 mm) expanded glass (EG) within an A356 alloy matrix. To this end, the counter-gravity infiltration casting technique is employed to manufacture the specimens. The density of the MSFs ranges from 1.05 to 1.17 g/cm^3, making it one of the lowest densities foams, attributed to the filler particles' low bulk density. The study investigates the influence of T6 heat treatment on the mechanical properties and microstructural characteristics of the manufactured MSFs. The mechanical properties of the MSFs are characterized under quasi-static compressive loads at 1 mm/min. After heat treatment, the compression test results indicate a significant enhancement in most mechanical properties. Compression strength and plateau stress are approximately doubled compared to as-cast foams for samples with similar densities. While energy absorption of the MSFs triples in heat-treated conditions. These improvements are attributed to changes in the matrix microstructure due to thermal treatment. Microstructural analysis reveals that Si particles, initially sharp and continuous within inter-dendritic boundaries, become blurry and discontinuous through spheroidization after thermal treatment. This hinders crack growth in the cell wall and mitigates the effects of casting defects and the columnar dendritic structure. The majority of mechanical properties in both heat-treated (HT) and as-cast (AC) foams exhibited an increase in density due to an increase in the matrix fraction. However, plateau end strain and energy absorption efficiency demonstrated an independent effect of heat treatment and density.

Keywords: Metal syntactic foam, mechanical properties, microstructure properties, expanded glass particle, A356 matrix, infiltration method

1.0 INTRODUCTION

Metal Syntactic Foams (MSFs) are novel lightweight materials consisting of particles embedded in a metal matrix [1]. Recently, they have garnered significant interest due to their exceptional physical and mechanical properties, including low density, high-energy absorption, and a favorable strength-to-weight ratio [2] The unique properties of the MSFs necessitate further exploration of their mechanical

characteristics and the influence of processing factors, such as heat treatment and aging processes [3]. Weak particles, such as expanded glass (EG) [4], [5], expanded clay [6] pumice [7], and expanded perlite [8] particles serve as space holders in MSFs, imparting ductility and stable deformation compared to MSFs with high-strength particles [9]. The mechanical properties of the MSFs with low-strength particles primarily depend on the metal matrix type and the microstructure of this matrix [10]. Consequently, heat treatment applied to aluminum matrices, such as A356, can enhance the mechanical properties of the MSFs. Several studies have demonstrated that heat treatment is an effective approach to tailoring the mechanical properties of MSFs [5].

To date, limited research has investigated the effect of different heat treatment processes on the microstructure and mechanical properties of MSFs containing high-strength particles [3]. Notably, these investigations have yielded insignificant results regarding the impact of heat treatment processes on mechanical properties. This might be attributed to the strong dependence of the mechanical properties of these MSFs on the filler particles rather than the matrix materials. These syntactic foams exhibit immature cracks at the beginning stages of compression and are brittle fracture-susceptible [11, 12]. This restricts the foam's ability to absorb energy. Few studies have explored the effects of heat treatment on MSF containing low-strength porous particles, revealing that heat treatment is a highly effective approach for enhancing the mechanical properties of metal syntactic foams, particularly when the matrix material is heat-treatable [13]. Taherishargh *et al.* [14] fabricated an MSF using inexpensive and ultralightweight expanded perlite particles as filler and A356 alloy as a matrix. The produced foams significantly improved plateau stress and absorbed energy after heat treatment. The primary reason for this improvement lies in the alteration of the microstructure of the matrix material. Bolat *et al.* [13] Heat-treated MSF specimens demonstrate greater mechanical and energy absorption characteristics, regardless of the size of the particles, in comparison to their as-cast properties with similar or nearly identical density values.

Expanded glass particle (EG) stands out as one of the best options for creating lightweight metal foams with a uniformly distributed filler, owing to its low density and approximately spherical shape. Previous studies have explored EG-MSFs using A356 as an untreated metal matrix [15]. The study's output samples are regarded as some of the lightest metal syntactic foams, making them appropriate for various uses. The novelty of this project is to create lightweight material while maintaining its mechanical properties and improving its energy absorption. This material can be useful in numerous applications like impact absorbers. The main way to enhance the mechanical properties of metal syntactic foams made of weak filler particles is via a heat-treatment process [16, 17]. Therefore, the primary objective of this study is to investigate the consequences of heat treatment on the mechanical properties of an MSF made of EG as a filler and A356 as a matrix. It's important to note that the EG particle used in this work was provided by a different supplier than in previous studies [4, 18, 19]. As a result, this work will include some characterizations for this particle.

2.0 METHODOLOGY

2.1 Preparation of Metal Foam

The counter-gravity infiltration casting was employed to fabricate the MSF samples. The A356 aluminum alloy and EG particles were used as the matrix and fillers respectively. This casting technique was described in detail in our previous research [12]. The composition of the A356 alloy comprises 7.2 wt% Si, 0.4 wt% Mg, 0.1 wt% Fe, and 0.12 wt% Ti, as indicated by the supplier's material datasheet (Hayes Metals Pty Ltd., Riverstone NSW 2765, Australia). The matrix composition was additionally verified and confirmed at the Chemical Science Department Laboratory of the University of Thi-Qar through optical emission spectroscopy.

The EG particles utilized in the current research study were manufactured from recycled crashed glasses. The composition of the EG particle consists of 71 wt% SiO_2, 2 wt% Al_2O_3, 13 wt.% Na_2O, 1 wt.% K_2O, 8 wt.% CaO, 0.5 wt.% Fe_2O_3, 2 wt.% MgO, and 0.5 wt.% as trace elements (supplied by Liaver GmbH & Co. KG, Germany). The appearance of the EG particles is grey. These particles were produced in different particle sizes ranging from 0.1-8 mm, as illustrated in Figure 1a. Figure 1b shows the internal porous structure of the EG particles, which contain pores of various sizes and are characterized by a closed shell, and a semi-spherical morphology. Some small surface cavities with various sizes are also visible on the outer surface of the EG particles.

In the first step of manufacturing, the graphite mold was filled with 2-2.8 mm EG particles in approximately seven to eight equal steps. This procedure ensures a uniform distribution of the particles packed bed within the mold. A steel mesh was then placed on top of the filler particles to stabilize them and prevent their downward movement due to gravity.

A specific mass of the A356 ingot was placed in a cylindrical graphite pot (see Figure 2). The pot was then positioned within an electrical furnace and held at 700 °C for 20 minutes. Subsequently, after that, the pot was taken out of the furnace, and the filled mold was inverted and placed into the pot. A steel container was then positioned atop the mold to gather any extra melt through the infiltration process. Subsequently, the entire setup was returned to the furnace for five minutes to heat the particle packing,

enhancing the infiltration process and preventing the effects of the cold mold. This procedure follows the novel approach used by Al-sahlani [2] to mitigate EG shrinkage at temperatures above 600 °C. After 5 minutes, the entire setup was removed from the furnace. A 3 kg mass was placed on the steel container to push the filled mold down. As a result, the molten metal infiltrated in the counter-gravity direction, filling the channels between the EG particles. The assembly was then cooled in the air. The samples were then removed from the mold and underwent machining using a lathe machine to remove the steel mesh.

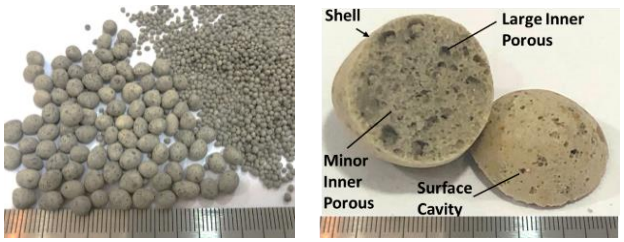

(a) Different sizes of EG (b) Cross section of EG.

Figure 1 Morphology and section of EG

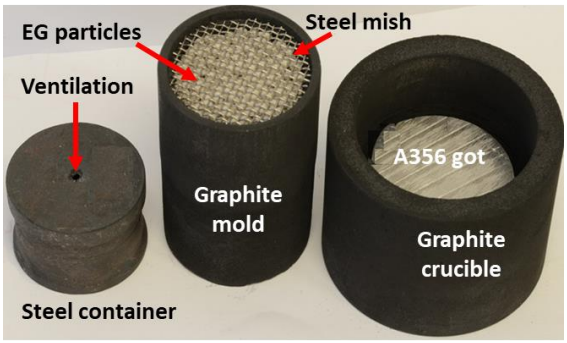

Figure 2 The setup of the counter-gravity pressure infiltration technique

2.2 Heat-treatment Method

The T6 heat-treatment procedure has been an effective procedure for improving the mechanical properties and microstructural features of the A356 aluminum alloy, as indicated by numerous studies published over the past decade [12,15]. In an extensive investigation, the influence of different solutions and aging durations on the mechanical characteristics of A356 alloy was examined by Tiryakioglu *et al*. [13]. The solution and aging times ranged from 1 to 64 hours and 1 to 30 hours, respectively. The best properties for strength are always possessed by A356 in the T6 approach [24, 25]. According to previous research studies [4,13, 14,15,17], the heat-treatment procedure depicted in Figure 3 was employed in the current study to achieve the optimal mechanical properties of the A356 aluminum alloy matrix. In this regard, the specimens underwent solution treatment at 540 °C for 16 hours and were subsequently cooled in agitated ice water. Following that, the specimens were artificially aged at 160 °C for 10 hours and cooled slowly in the air.

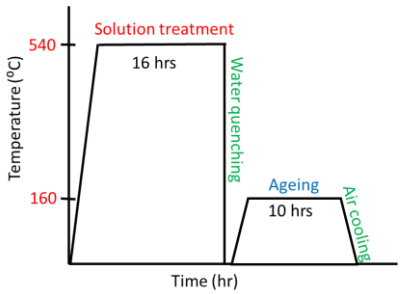

Figure 3 T6 heat-treatment approach

2.3 Microstructure Characterization

In order to examine the aluminum syntactic foams' microstructure, an Olympus BX60M optical microscope was used. Two slices from both untreated and heat-treated samples were cut for typical grinding and polishing. The sections were mounted with resin and polished using grit silicon carbide papers of varying grades. Succeeding polishing with 6 µm and 1 µm diamond suspensions in distilled water was performed to attain a high-quality surface finish for microscopic observations. After utilizing an ultrasonic cleaner for 20 minutes to eliminate unwanted micronized contaminants, the samples were dried in an oven for 24 hours.

2.4 Compression Tests

The physical characteristics of the MSF samples, including their mass (m_{MSF}), diameter (D) and height (H) were calculated. Then, the volume of each MSF (V_{MSF}) and its density (ρ_{MSF}), in as cast and heat-treated conditions were determined using equations (1) and (2) respectively:

$$V_{MSF} = \left(\frac{\pi D^2}{4}\right) * H \quad \text{.....(1)}$$

$$\rho_{MSF} = \frac{m_{MSF}}{V_{MSF}} \quad \text{.....(2)}$$

Equations provided by Taherishargh [27] are employed to mathematically determine the volume fraction of EG particles (F_P) and total porosity percentage of the samples (F_T). In these equations, (m_P) and (V_P) represent the mass and volume of the EG particle filler, respectively. Additionally, (ρ_P) and (ρ_S) denote the particle density and solid state of the EG spheres respectively, while (ρ_{Al}) is the density of the matrix.

$$V_P = V_{MSF} - \frac{m_{MSF} - m_P}{\rho_{Al}} \quad \text{.....(3)}$$

$$F_P = \frac{V_P}{V_{MSF}} \quad \text{.....(4)}$$

$$\rho_P = \frac{m_P}{V_P} \quad \text{.....(5)}$$

$$F_T = F_P * (1 - \frac{\rho_P}{\rho_S}) \quad \text{.....(6)}$$

A uniaxial computer-controlled 50 kN Shimadzu testing machine was utilized to conduct quasi-static compression tests on both groups of samples. This test determines the mechanical properties of the MSFs. To minimize frictional effects, a silicone release agent was sprayed onto the surfaces of the compression test platens to lubricate them. The samples were compressed at a constant crosshead speed of 1 mm/min. The load-displacement data was recorded during the test using the machine software (Trapezium 2). The initial cross-sectional area and height of the samples were used to derive the engineering stress-strain curves $(\sigma - \varepsilon)$.

ISO 13314 standard [28] was used to determine the mechanical properties of the MSF samples. According to this standard, the initiation of plastic deformation is estimated by determining the 1% offset yield stress. The plateau stress (σ_{pl}) of the MSFs was determined as the arithmetic stress value in the strain range of 0.2-0.4. The volumetric energy absorption capacity (*W*) of the metal foam samples is represented by the area under the stress-strain curve up to the strain value of 0.5. This can be calculated according to equation (7)

$$W = \int_0^{e_{50\%}} \sigma de \quad \text{.....(7)}$$

where σ and e are the compressive stress and strain, respectively.

The energy absorption efficiency (η), which represents the proportion of actual to ideal energy absorption of MSF, is another important material factor in metal foams. This parameter can be calculated according to equation (8) below and shows the uniformity of the stress within the stress-strain curve up to the strain value of 0.5:

$$\eta = \frac{W}{\sigma_{max}\, e_{50\%}} \quad \text{.....(8)}$$

where σ_{max} is the foam's maximum stress up to 50% strain.

3.0 RESULTS AND DISCUSSION

3.1 Particle Characters

The EG particle used in this research was supplied by Liaver Company. It is grey, and its chemical composition is slightly different from the EG provided by Poraver Company (see section 2.1), which was used in previous works [4, 18, 19, 25]. The current EG exhibited a higher softening point than the previous one, resulting in less particle shrinkage when heated above 600 °C, which is likely due to variations in composition. Other physical properties, such as shape and bulk density (measured using the method explained in [2]), are comparable and fall within the range of 0.19-0.20 g/cm^3 [18].

SEM tests were conducted on the EG particles to investigate their structure. The results showed that the inner structure of the spheres consists of a wide range of porous sizes separated by struts, as depicted in Figure 4a. The shell and struts are also formed with multiple tiny pores. A higher magnification of the particles revealed that the shell has variable thickness and various sizes of small pores (1 – 200 µm), as shown in Figure 4b. A similar observation was made by [29]. This finding explains the closed-cell morphology of the EG particles, despite having some surface holes. This characteristic, combined with its relatively high crushing strength [18] makes EG particles an excellent candidate to be used as filler for manufacturing different MSF

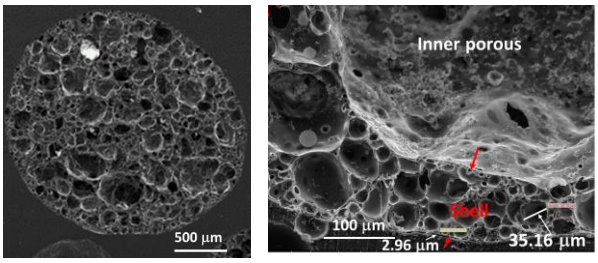

(a) Whole section (b) the shell microstructure

Figure 4 The internal structure of EG

3.2 Structural Characteristics of MSF

Figure 5a shows a manufactured sample of MSF and its morphology. To characterize the manufactured EG MSFs, a cross-section of a sample was prepared and investigated in this research. Figures 5b illustrate a typical macrostructure of the fabricated MSFs. All samples demonstrate excellent aluminum matrix distribution and harmony, attributed to the greater infiltration ability of the counter-gravity pressure infiltration technique. No signs of unintended aluminum melt infiltrating into particles during the production process or particle breakage were observed; all particles remained intact.

Figure 5c shows a scanning electron microscope (SEM) image of the magnified area of the section. In this Figure, it is evident that the particle retains its spherical shape despite the high temperature during the process. This preservation is achieved through the technique used to control EG particle shrinkage [18]. Additionally, there are numerous small inter-particle voids located in proximity to the contact areas between adjacent particles, where the melt failed to fill these narrow channels. These voids are indicated by white arrows in Figure 5b. Void patches create

specific vulnerabilities in the foam and could serve as a precursor to larger-scale collapse. This is described in more detail in [18].

The microscope images in Figures 6a and 6b show other types of voids or micropores resulting from casting defects or solidification shrinkage. These defects are indicated by white arrows in the figures. The volume contraction accompanying dendritic solidification led to shrinkage, resulting in the development of small casting defects [30]. However, poor feeding or lack of infiltration is the main reason for the formation of large casting defects occurring in the matrix in the narrow interspace of touching EG particles. Similar findings are documented in research on solid A356 alloy [31]. These types of porosities weaken the MSFs and decrease their strength during the loading tests. Figures 6a and 6b display the characteristic microstructure of the as-cast EG/A356 MSF. The metal alloy matrix consists of a network of primary and secondary dendritic arms that are rich in aluminum. A eutectic structure, comprising silicon and aluminium-rich phases, is disorderly distributed in the dendritic boundaries of the grains [31]. The silicon phase develops with morphologies resembling rods or plates [32]. The dominant structure in the cell walls of MSFs is the columnar dendritic grain morphology.

(a) MSF sample

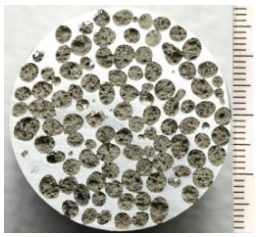

(b) MSF sample section

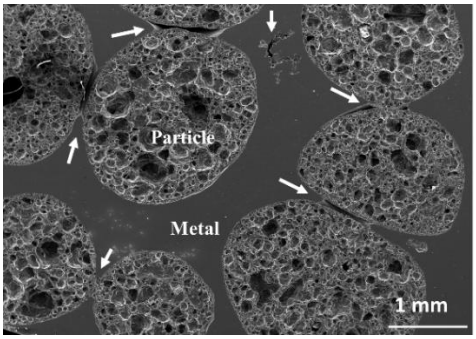

(c) SEM of interparticle matrix and particle

Figure 5 The macrostructure of the EG MSF sample

Dendrites begin to nucleate at the EG particle surface, creating a columnar dendritic structure in different sizes. Typically, one direction of dendritic growth predominates over the others most of the time. In the narrow interparticle spaces, the entire grain microstructure is affected by nucleation around the particle (Figure 6b). Nucleation signifies good wettability between the aluminum melts and EG particles. In the wide interparticle spaces and in areas far from the particle surface, dendrites also grow in approximately columnar arms with different directions (Figure 6a). Similar observations on the solidification structure of Mg-based syntactic foams have been documented in [33].

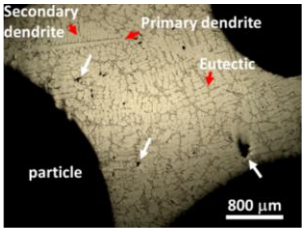

(a) Small casting defect via optical microscope

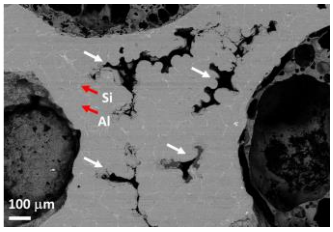

(b) Large casting defect in the cell wall via SEM

Figure 6 The microstructure of as-cast EG/A356 MSF

Figure 7a shows the high magnification of the microstructure of the matrix in the as-cast foam sample. This microstructure consists of primary and secondary aluminium dendrites bounded by a sharp continuous eutectic Si, as explained above. The matrix microstructure of the heat-treated MSF sample is presented in Figure 7b. The heat treatment process significantly alters the morphology of the Si-rich network but does not affect the dendritic structure of the matrix. Under heat-treated conditions, the sharp continuous network of the Si phase in the as-cast matrix changes to a discontinuous clouding network. This change is a result of the heat treatment process causing the Si phase to change in size and shape. The majority of eutectic Si has granular shapes and is discontinuously distributed on the grain boundaries. Several studies have reported that the Si phase becomes approximately spherical and spherically expands at high temperatures [21, 34, 35]. This is observed in Figure 7b. The size of the aluminum dendrites in the heat-treated matrix becomes finer than that in the as-cast cell wall due to the effect of heat treatment. Studies reveal that the microstructure of binary phase alloys can change due to convection in the melt or changes in temperature gradient during solidification [36].

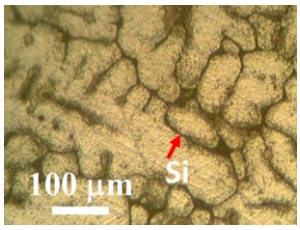

(a) As-cast sample

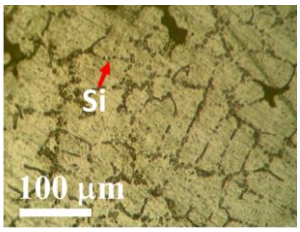

(b) Treated sample

Figure 7 The microstructure of EG A356

According to several studies [22, 34], Mg-rich phases dissolve, and alloying elements like Mg and Si become homogenized during the solution treatment. During the stage of artificial aging, dissolved elements precipitate. The precipitates and eutectic Si are the main sources of alloy matrix strengthening in the A356 material. Si atom clustering initiates the precipitation, followed by the creation of different phases that end with the stable phase of Mg_2Si. Due to their tiny size (smaller than 500 nm), the Mg_2Si needles are hardly visible under optical microscopy [22]. This explains the eutectic changes after the heat-treated solution and/or aging approach.

3.3 Physical Properties of Produced MSF

Table 1 shows the main physical properties of the heat-treated foams. HTEG-MSF stands for heat-treated expanded glass metal syntactic foams. After measuring the height of the samples with approximately constant diameter (28.5 mm), the volume of each sample was calculated according to Equation 1. The mass of each sample was measured using a digital accurate scale. Thus, the density of each sample can be calculated according to Equation 2. The volume fraction of filler particles (F_P), the volume of filler (V_P) and total porosity percentage (F_T) of each sample were estimated using equations 3-6. The results are presented in Table 1.

The average foam density of all heat-treated samples is 1.13 g/cm³. The lowest density is 1.06 g/cm³, which was for sample 1 (HTEG-MSF1). This means that the produced foam in this research has one of the lowest densities compared to previous literature efforts. Broxtermann [37]and Taherishargh [27, 38] made MSF considered the lowest densities among aluminum syntactic foams, 0.75 and 1.05 g/cm³, respectively. EG particles are very lightweight porous particles with a solid and closed shell. Its density is close to the density of expanded perlite, which is considered the lightest porous particle [27]. EG has a reasonable crush resistance to resist pressure or metal leakage during fabrication processes [25]. According to Table 1, the average volume fraction of EG filler for all samples is 65.4%, which is considered one of the highest filler volume fractions compared to [27].

Table 1 Physical characteristics of AC- [9] and HT-MSF

MSF	m_{MSF} g	H cm	V_P cm³	ρ_{MSF} g/cm³	F_P %	F_T %
HT1	25.00	37.00	23.59	1.06	67.97	60.81
HT2	28.09	39.00	24.87	1.13	65.38	58.20
HT3	28.57	39.44	25.15	1.14	65.14	57.95
HT4	29.58	40.30	25.70	1.15	64.58	57.39
HT5	30.63	41.5	26.46	1.16	64.33	57.15
AC1	23.86	40.05	22.41	1.05	67.74	60.62
AC2	23.98	40.22	22.51	1.05	67.71	60.59
AC4	22.48	35.5	19.87	1.13	65.24	58.12
AC3	24.71	37.7	21.10	1.17	63.76	56.64

The average porosity of these produced foams is 58.3%. This suggests that the technique used to manufacture the foam samples and the method of batching the filler in the mold [18] were effective in preventing penetration of molten metal or leakage. Compared to other publications [18, 27], the value of porosity (F_T) a be considered one of the highest porosities. In comparison to as-cast samples from [18], the T6 heat treatment process did not change the physical properties of the samples.

3.4 Experimental Compressive Testing

Figure 8 displays the compressive stress-strain curves of T6 heat-treated metal syntactic foams (HT-MSFs). The stress-strain curves of four as-cast foams (AC-MSFs) from [18] which have comparable densities of 1,05, 1.13, and 1,14 kg/cm³, are included in Figure 9 for comparison. All curves illustrate a typical system for cellular metals, comprising a linear elastic section, the plateau section, and the densification area [25, 27]. After an elastic region, all curves exhibit slight fluctuations throughout the plateau region. The AC curves progressively decline continuously, indicating progressive plastic deformation. Nonetheless, each HT foam demonstrates a consistent stress escalation up to around 35% strain. Following this point, a majority of them initiate a gradual decline accompanied by significant fluctuations. A consistent, uniform layer-by-layer foam deformation in ductile behavior is the main reason for the progressively increasing stress-strain curve of HT samples [14]. After that, shear bands separate through the whole sample, leading to a decline in the stress-strain curve due to an increase in collapsed cell walls. This holds true for all HT curves except for the heat-treated sample (HT-MSF1) with the lowest density, which continues to exhibit a steadily increasing stress throughout the entire plateau area. Tahershargh [27, 37] showed similar observations. The reason for this can be explained according to the deformation mechanism. The influence of shear bands exhibited a limited impact on the given sample. It is likely because this sample has more porosity than others (less density), which can lead to more space for cell walls to deform. The heightened ductility observed in the cell wall of HT foams, coupled with the delayed collapse of cells in regions experiencing maximum shear stress, remains a potential contributing factor. This phenomenon persists, even in samples featuring thinner walls. Accordingly, it is possible to argue that the heat treatment produces uniform deformation characteristics that are desirable.

When high energy absorption is required, plateau stress value is crucial for metal syntactic foams. The final stage sees a sudden upsurge in the stress value as the majority of the space holder (EG particles) collapse. It is evident from Figure 8 that heat treatment significantly enhances the strength of EG-MSFs. This improvement is attributed to the changes

in the microstructure of the matrix cell walls of MSFs, as explained in section 3.2.

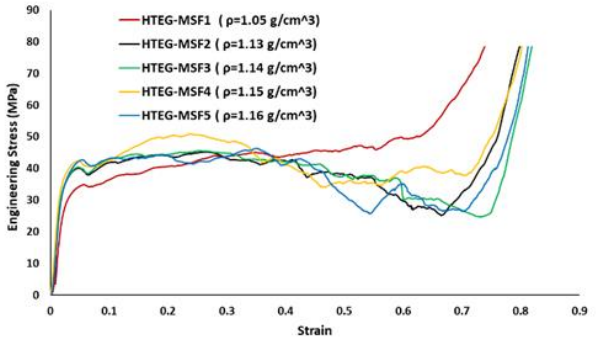

Figure 8 Compressive stress-strain curves of as-cast metal syntactic foams [18].

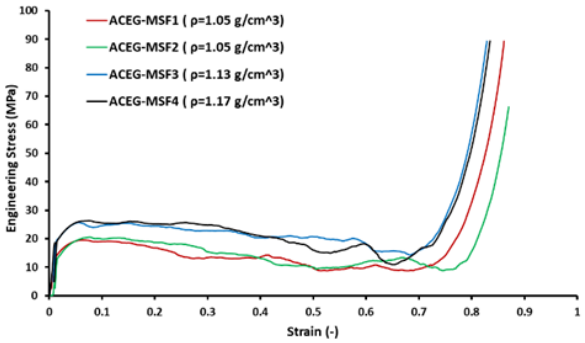

Figure 9 Compressive stress-strain curves of heat-treated metal syntactic foams

Table 2 summarizes the important mechanical characteristics of HT-MSF samples resulting from the compressive test. However, the results of AC-MSF samples were obtained from [18]. The 1% compression stress (σ_c), plateau stress (σ_{pl}), plateau end strain (ε_{pl}), energy absorption (W), and energy absorption efficiency values (η) resulting from stress-strain curves of samples were computed according to the ISO13314 standard [28] (equation 7 and 8) and are presented in this Table.

According to the literature [14, 26, 39], heat treatment of solid A356 alloy substantially improves its mechanical properties. Similarly, heat treatment of metal syntactic foams made of weak particles enhances the mechanical characteristics since most of the compressive force is supported by the matrix structure [13, 34, 35, 40, 41]. Except for plateau end strain, all mechanical properties of HTEG-MSFs samples are substantially higher than those of ACEG-MSFs at near-density value (see Table 2).

The heat-treated syntactic foams show higher compression strength values compared to as-cast foams at near-density values. The average strength values of HT and AC samples are 35.8 and 18.2 MPa, respectively (see Figure 10 a). This means that the heat-treated foams doubled in compression strength which is a phenomenal increase in strength. EG particles are weak to support the compression load as a filler.

Table 2 Mechanical properties of as-cast and heat-treated MSFs

MSF	ρ g/cm³	σ_c MPa	σ_{pl} MPa	ε_p –	W MJ/m³	η –
HT1	1.06	31.11	56.45	0.654	27.67	0.87
HT2	1.13	36.01	56.36	0.769	29.61	0.91
HT3	1.14	36.11	57.21	0.793	30.56	0.92
HT4	1.15	38.47	61.60	0.779	32.97	0.85
HT5	1.16	37.28	56.46	0.784	29.64	0.89
AC1	1.05	15.31	18.03	0.765	10.28	0.77
AC2	1.05	15.70	20.74	0.809	11.60	0.78
AC4	1.13	20.81	31.37	0.767	16.08	0.88
AC3	1.17	21.03	29.54	0.755	16.06	0.88

A major characteristic of MSFs that is critical to their ability to absorb energy and withstand deformation during wide-strain compression is plateau stress. The plateau stress of HTMSF1 with a density of 1.06 g/cm³ (27.67 MJ/m³) is approximately 2.4 times higher than the plateau stress of ACMSF1 with a closed density (10.28 and 11.60 MJ/m³). This result can be one of the best improvements in the plateau stress of MSFs [14, 37]. According to Table 2 and Figure 10 b, the average plateau stress value of heat-treated MSFs (57.6 MPa) is remarkably higher than that of as-cast samples (24.9 MPa).

Similarly, heat-treated MSFs exhibit a significant improvement in energy absorption capacity in comparison to as-cast. The primary criteria used to assess metallic foams' energy absorption capacity are their efficiency and capacity. The average energy absorption value of HT foams is 30 MPa, which is about 124% higher than the average value of AC foams (see Figure 10 c). This remarkable improvement is due to the high compression stress of HT foams, although there is a reduction in the matrix ductility.

The maximum energy absorption efficiency for HT foam is 91%, while for AC, it is around 88% (see Table 2 and Figure 10 d). This means that the efficiency is hardly improved after T6 heat treatment since it is dependent upon the ideal flat behaviour of the plateau zone and filler characteristics such as shape and pore style. HT3 sample showed the highest efficiency because it is the most flattened curve (see Figure 8) and the longest plateau strain as shown in Figure 10 e. Correspondingly, no obvious impact of heat treatment on the value of plateau strain was found. For T6 HT and AC foams, the average plateau end strain values are very close; they are 0.76 and 0.77 respectively (see Figure 10 e).

In a prior study [14, 19], it was demonstrated that the matrix controls the mechanical properties of the metal syntactic foam and that the lightweight porous particles do not directly improve those properties. However as explained in Section 3.2, the EG particles induce some changes in the cell wall microstructure by developing a columnar dendritic structure (see Figure 7b). With this structure, the mechanical characteristics of the cell walls are not isotropic and are negatively impacted. Along the dendritic arms, the cell wall's mechanical properties are greater; in other directions, they are lower. The explanation for this is that failure begins at the inter-dendritic boundaries, which are susceptible to crack initiation due to a continuous network of flake-like Si particles. The total area of the inter-dendritic boundaries is greater in directions other than the direction of dendritic dominance. The condensed Si particle network and its distinct boundaries are blurred by the heat treatment (see Figure 7b). The growth of cracks is limited by the spheroidized Si particles with a significant interparticle distance. Therefore, by enhancing conditions in directions other than the prominent dendritic direction, heat treatment can be used to mitigate the negative effects of the columnar dendritic structure on the mechanical properties of the cell wall.

Primarily, the mechanical characteristics of HT- and AC-MSFs samples are significantly influenced by density, as depicted in Figure 10. The impact of density on compression strength, energy absorption, and plateau stress in both HT and AC samples follows a similar trend, increasing with density (refer to Figure 10 and Table 2). Notably, differences in mechanical properties are observed among foams with the same or close density. These variations are attributed to cell wall microstructure, imperfections, and pore structure [42]. Refining the microstructure of cell walls during heat treatment has led to a reduction in the effect of imperfections in the cell walls. According to the experimental findings, the energy absorption efficiency and plateau end strain of MSFs are independent parameters unrelated to foam density, as previous studies have found [18, 43]

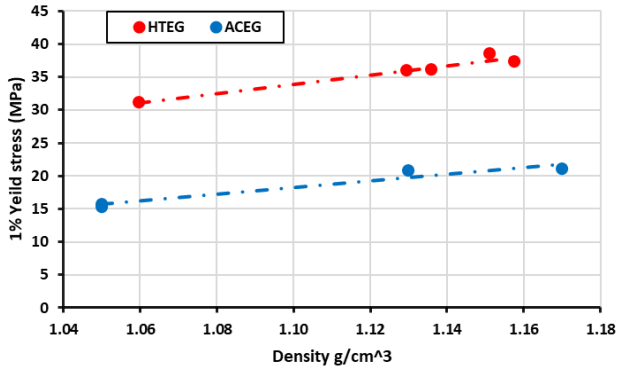

(a) Compression strength

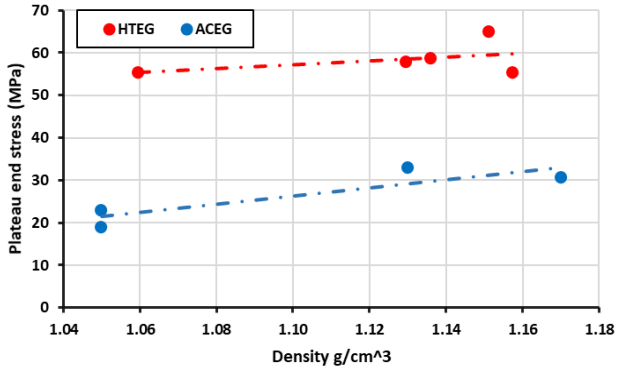

(b) Plateau stress

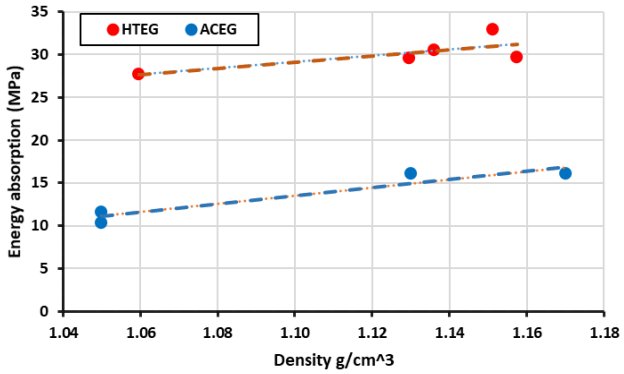

(c) Energy absorption

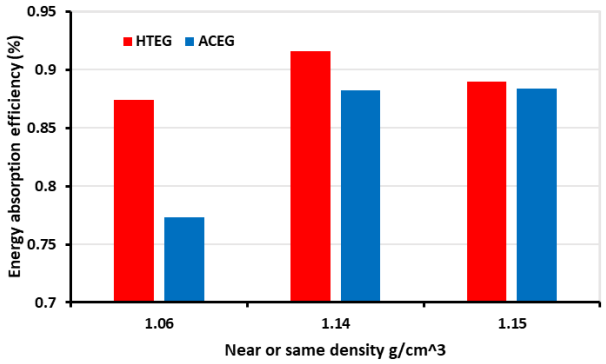

(d) Energy efficiency

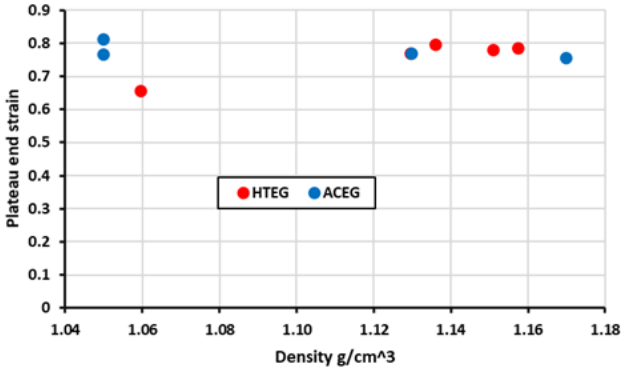

(e) Plateau end strain

Figure 10 The mechanical properties of HT and AC metal syntactic foams

4.0 CONCLUSION

This experimental study focused on the impact of T6 heat treatment on the mechanical characteristics of EG/A356 syntactic foams leading to the following key findings from compression tests and microstructural observations. First of all, the counter gravity low-pressure infiltration process was successfully used to produce EG/A356 foams with a good filler distribution. The investigation revealed a high porosity ranging between 64% and 68%, considered among the highest porosities of MSFs. T6 heat treatment changed the microstructure of the Al columnar dendrite structure that was formed near the surface of EG particles. Also, heat treatment altered the microstructure by blurring and spheroidizing the continuous and sharp network of silicon phases in the eutectic structure, leading to an increase in the aspect ratio and interparticle distance of Si particles. This microstructural change delays the shear band and increases the ductility of the HT A356 matrix, resulting in significant improvements in mechanical characteristics.

The stress-strain curves of the heat-treated MSFs exhibited a typical behavior with a small elastic area, large plateau region, and densification. The mechanical characteristics of the HT-MSFs, including compression strength, plateau stress, and absorption energy, were significantly increased compared to AC foams. The compression and plateau stresses of the HT foams were approximately twice as high as those of AC foams. The absorption energy increased around three times after heat treatment. In addition, the compression strength, energy absorption, and plateau stress were significantly influenced by density for both HT and AC samples. This indicates that the characteristics of the metal matrix regulate the majority of mechanical characteristic of EG/A356 foams. However, the energy absorption efficiency and plateau end strain were found to be independent of density and heat treatment.

Acknowledgement

We want to express our gratitude to the College of Engineering, The University of Thi-Qar for their helpful feedback and support.

Conflicts of Interest

The author(s) declare(s) that there is no conflict of interest regarding the publication of this paper.

References

[1] P. K. Rohatgi, N. Gupta, B. F. Schultz, and D. D. Luong. 2011. The Synthesis, Compressive Properties, and Applications of Metal Matrix Syntactic Foams. *JOM*. 63(2): 36–42. Doi: 10.1007/s11837-011-0026-1.

[2] A. Kennedy. 2012. Porous Metals and Metal Foams Made from Powders. [Online]. Available: www.intechopen.com.

[3] I. N. Orbulov and J. Ginsztler. 2012. Compressive Characteristics of Metal Matrix Syntactic Foams. *Compos Part A Appl Sci Manuf*. 43(4): 553–561. Doi: 10.1016/j.compositesa.2012.01.008.

[4] T. Fiedler, K. Al-Sahlani, P. A. Linul, and E. Linul. 2020. Mechanical Properties of A356 and ZA27 Metallic Syntactic Foams at Cryogenic Temperature. *J Alloys Compd*. 813. Doi: 10.1016/j.jallcom.2019.152181.

[5] A. Wright and A. Kennedy. 2017. The Processing and Properties of Syntactic Al Foams Containing Low Cost Expanded Glass Particles. *Adv Eng Mater*. 19(11). Doi: 10.1002/adem.201600467.

[6] I. N. Orbulov, A. Szlancsik, A. Kemény, and D. Kincses. 2020. Compressive Mechanical Properties of Low-cost, Aluminium Matrix Syntactic Foams. *Compos Part A Appl Sci Manuf*. 135: 105923. Doi: 10.1016/j.compositesa.2020.105923.

[7] M. Taherishargh, I. V. Belova, G. E. Murch, and T. Fiedler. 2015. Pumice/aluminium Syntactic Foam. *Materials Science and Engineering: A*. 635: 102–108. Doi: 10.1016/j.msea.2015.03.061.

[8] M. Taherishargh, E. Linul, S. Broxtermann, and T. Fiedler. 2018. The Mechanical Properties of Expanded Perlite-aluminium Syntactic Foam at Elevated Temperatures. *J Alloys Compd*. 737: 590–596. Doi: 10.1016/j.jallcom.2017.12.083.

[9] A. Kemény, N. Movahedi, T. Fiedler, J. E. Maróti, and I. N. Orbulov. 2022. The Influence of Infiltration Casting Technique on Properties of Metal Syntactic Foams and Their Foam-Filled Tube Structures. *Materials Science and Engineering: A*. 852: 143706. Doi: 10.1016/j.msea.2022.143706.

[10] N. Movahedi, G. E. Murch, I. V. Belova, and T. Fiedler. 2019. Functionally Graded Metal Syntactic Foam: Fabrication and Mechanical Properties. *Mater Des*. 168: 107652. Doi: 10.1016/j.matdes.2019.107652.

[11] X. F. Tao and Y. Y. Zhao. 2012. Compressive Failure of Al Alloy Matrix Syntactic Foams Manufactured by Melt Infiltration. *Materials Science and Engineering: A*. 549: 228–232. Doi: 10.1016/j.msea.2012.04.047.

[12] X. F. Tao and Y. Y. Zhao. 2009. Compressive Behavior of Al Matrix Syntactic Foams Toughened with Al Particles. *Scr Mater*. 61(5): 461–464. Doi: 10.1016/j.scriptamat.2009.04.045.

[13] Ç. Bolat, İ. C. Akgün, and A. Gökşenli. 2022. Effect of Aging Heat Treatment on Compressive Characteristics of Bimodal Aluminum Syntactic Foams Produced by Cold Chamber Die Casting. *International Journal of Metalcasting*. 16(2): 646–662. Doi: 10.1007/s40962-021-00629-0.

[14] M. Taherishargh, I. V. Belova, G. E. Murch, and T. Fiedler. 2014. On the Mechanical Properties of Heat-treated Expanded Perlite-aluminium Syntactic Foam. *Mater Des*. 63: 375–383. Doi: 10.1016/j.matdes.2014.06.019.

[15] E. Linul, D. Lell, N. Movahedi, C. Codrean, and T. Fiedler. 2019. Compressive Properties of Zinc Syntactic Foams at Elevated Temperatures. *Compos B Eng*. 167: 122–134. Doi: 10.1016/j.compositesb.2018.12.019.

[16] N. Movahedi, G. Murch, I. Belova, and T. Fiedler. 2019. Effect of Heat Treatment on the Compressive Behavior of Zinc Alloy ZA27 Syntactic Foam. *Materials*. 12(5): 792. Doi: 10.3390/ma12050792.

[17] I C Akgün, C. ¸ Bolat, and A. G. Gök¸senli. 2021. Effect of Aging Heat Treatment on Mechanical Properties of Expanded Glass Reinforced Syntactic Metal Foam. *Konvove Mater*. 59: 345–355. Doi: 10.4149/km.

[18] K. Al-Sahlani, M. Taherishargh, E. Kisi, and T. Fiedler. 2017. Controlled Shrinkage of Expanded Glass Particles in Metal Syntactic Foams. *Materials*. 10(9). Doi: 10.3390/ma10091073.

[19] K. Al-Sahlani, S. Broxtermann, D. Lell, and T. Fiedler. 2018. Effects of Particle Size on the Microstructure and

Mechanical Properties of Expanded Glass-metal Syntactic Foams. *Materials Science and Engineering: A*. 728. Doi: 10.1016/j.msea.2018.04.103.
[20] K. T. Akhil, S. Arul, and R. Sellamuthu. 2014. The Effect of Heat Treatment and Aging Process on Microstructure and Mechanical Properties of a356 Aluminium Alloy Sections in Casting. *Procedia Engineering*. 1676–1682. Doi: 10.1016/j.proeng.2014.12.318.
[21] M. Tiryakioglu. 2006. The Effect of Solution Treatment and Artificial Aging on the Work Hardening Characteristics of a Cast Al–7%Si–0.6%Mg Alloy. *Material Science and Engineering*. 427: 154–159.
[22] J. Peng, X. Tang, J. He, and D. Xu. 2011. Effect of Heat Treatment on Microstructure and Tensile Properties of A356 Alloys. *Transactions of Nonferrous Metals Society of China*. 21(9): 1950–1956. Doi: 10.1016/S1003-6326(11)60955-2.
[23] D. A. Lados, D. Apelian, and L. Wang. 2011. Aging Effects on Heat Treatment Response and Mechanical Properties of Al-(1 to 13 pct) Si-Mg Cast Alloys. *Metallurgical and Materials Transactions B*. 42(1): 181–188. Doi: 10.1007/s11663-010-9438-5.
[24] G. Liu, J. Gao, C. Che, Z. Lu, W. Yi, and L. Zhang. 2020. Optimization of Casting Means and Heat Treatment Routines for Improving Mechanical and Corrosion Resistance Properties of A356-0.54Sc Casting Alloy. *Mater Today Commun*. 24: 101227. Doi: 10.1016/j.mtcomm.2020.101227.
[25] K. Al-Sahlani, E. Kisi, and T. Fiedler. 2019. Impact of Particle Strength and Matrix Ductility on the Deformation Mechanism of Metallic Syntactic Foam. *J Alloys Compd*. 786. Doi: 10.1016/j.jallcom.2019.01.283.
[26] L. BoChao, P. YoungKoo, and D. HongSheng. 2011. Effects of Rheocasting and Heat Treatment on Microstructure and Mechanical Properties of A356 Alloy. *Materials Science and Engineering: A*. 528(3): 986–995. Doi: 10.1016/j.msea.2010.09.059.
[27] M. Taherishargh, I. V. Belova, G. E. Murch, and T. Fiedler. 2014. Low-density Expanded Perlite–aluminium Syntactic Foam. *Materials Science and Engineering: A*. 604: 127–134. Doi: 10.1016/j.msea.2014.03.003.
[28] ISO standard. 2011. Compression Test for Porous and Cellular Metals. *Mechanical Testing of Metals*. 13314. Switzerland
[29] M. Su, H. Wang, H. Hao, and T. Fiedler. 2020. Compressive Properties of Expanded Glass and Alumina Hollow Spheres Hybrid Reinforced Aluminum Matrix Syntactic Foams. *J Alloys Compd*. 821: 153233. Doi: 10.1016/j.jallcom.2019.153233.
[30] G. Nicoletto, R. Konečná, and S. Fintova. 2012. Characterization of Microshrinkage Casting Defects of Al–Si Alloys by X-ray Computed Tomography and Metallography. *Int J Fatigue*. 41: 39–46. Doi: 10.1016/j.ijfatigue.2012.01.006.
[31] K. Lee, Y. N. Kwon, and S. Lee. 2008. Effects of Eutectic Silicon Particles on Tensile Properties and Fracture Toughness of A356 Aluminum Alloys Fabricated by Low-Pressure-casting, Casting-forging, and Squeeze-casting Processes. *J Alloys Compd*. 461(1–2): 532–541. Doi: 10.1016/j.jallcom.2007.07.038.
[32] M. O. Shabani, A. Mazahery, A. Bahmani, P. Davami, And N. Varahram. 2011. Solidification of A356 Al Alloy: Experimental Study and Modeling. *Metallic Materials*. 49(04): 253–258. Doi: 10.4149/km_2011_4_253.
[33] A. Daoud, M. Abouelkhair, M. Abdelaziz, And P. Rohatgi. 2007. Fabrication, Microstructure and Compressive Behavior of ZC63 Mg–microballoon Foam Composites. *Compos Sci Technol*. 67(9): 1842–1853. Doi: 10.1016/j.compscitech.2006.10.023.
[34] Y. Harada, S. Tamura, and S. Kumai. 2011. Effects of High-Temperature Solutionizing on Microstructure and Tear Toughness of A356 Cast Aluminum Alloy. *Mater Trans*. 52(5): 848–855. Doi: 10.2320/matertrans.L-MZ201105.
[35] M. Zhu, Z. Jian, G. Yang, and Y. Zhou. 2012. Effects of T6 Heat Treatment on the Microstructure, Tensile Properties, and Fracture Behavior of the Modified A356 Alloys. *Materials & Design (1980-2015)*. 36: 243–249. Doi: 10.1016/j.matdes.2011.11.018.
[36] J. A. Sekhar and R. Trivedi. 1991. Solidification Microstructure Evolution in the Presence of Inert Particles. *Materials Science and Engineering: A*. 147(1): 9–21. Doi: 10.1016/0921-5093(91)90800-3.
[37] S. Broxtermann, M. Taherishargh, I. V. Belova, G. E. Murch, and T. Fiedler. 2017. On the Compressive Behaviour of High Porosity Expanded Perlite-Metal Syntactic Foam (P-MSF). *J Alloys Compd*. 691: 690–697. Doi: 10.1016/j.jallcom.2016.08.284.
[38] M. Taherishargh, I. V. Belova, G. E. Murch, and T. Fiedler. 2017. The Effect of Particle Shape on Mechanical Properties of Perlite/Metal Syntactic Foam. *J Alloys Compd*. 693: 55–60. Doi: 10.1016/j.jallcom.2016.09.168.
[39] H. Azimi, S. Nourouzi, and R. Jamaati. 2021. Effects of Ti Particles and T6 Heat Treatment on the Microstructure and Mechanical Properties of A356 Alloy Fabricated By Compocasting. *Materials Science and Engineering: A*. 818: 141443. Doi: 10.1016/j.msea.2021.141443.
[40] Ç. Bolat, G. Bilge, and A. Gökşenli. 2021. An Investigation on the Effect of Heat Treatment on the Compression Behavior of Aluminum Matrix Syntactic Foam Fabricated by Sandwich Infiltration Casting. *Materials Research*. 24(2). Doi: 10.1590/1980-5373-mr-2020-0381.
[41] L. Pan *et al.* 2018. Zn-matrix Syntactic Foams: Effect of Heat Treatment on Microstructure and Compressive Properties. *Materials Science and Engineering: A*. 731: 413–422. Doi: 10.1016/j.msea.2018.06.072.
[42] X. Xia, W. Zhao, X. Feng, H. Feng, and X. Zhang. 2013. Effect of Homogenizing Heat Treatment on the Compressive Properties of Closed-cell Mg Alloy Foams. *Mater Des*. 49: 19–24. Doi: 10.1016/j.matdes.2013.01.064.
[43] D. K. Balch, J. G. O'Dwyer, G. R. Davis, C. M. Cady, G. T. Gray, and D. C. Dunand. 2005. Plasticity and Damage in Aluminum Syntactic Foams Deformed under Dynamic and Quasi-Static Conditions. *Materials Science and Engineering: A*. 391(1–2): 408–417. Doi: 10.1016/j.msea.2004.09.012.